*Progress In Electromagnetics Research B, Vol. 39, 301–318, 2012*

# DESIGN AND FABRICATION OF RF-MEMS SWITCH FOR V-BAND RECONFIGURABLE APPLICATION

**T. M. Vu[1, 2, *], G. Prigent[1, 2], J. Ruan[3, 4], and R. Plana[3, 4]**

[1]University of Toulouse, INPT, UPS, LAPLACE, ENSEEIHT, 2 rue Charles Camichel, BP 7122, F-31071 Toulouse, France

[2]CNRS, LAPLACE, F-31071 Toulouse, France

[3]CNRS, LAAS, 7 avenue du Colonel Roche, F-31077 Toulouse, France

[4]University of Toulouse, UPS, INSA, INP, ISAE, LAAS, F-31077 Toulouse, France

**Abstract**—This paper presents a study of RF MEMS switch designed to be integrated in tunable filters for applications from W-frequency band to V-frequency band. Along the whole process, we go into detail of each procedure to present a complete study from design to fabrication and characterization of a RF-MEMS switch. The proposed concepts are validated by experimental results.

## 1. INTRODUCTION

The increasing demand for compact and low cost communication systems has generated the development of single devices operating at multiple frequency bands that can reduce manufacturing cost and space occupation. In general, to develop an electrically reconfigurable device, active switching or tuning elements such as semiconductor varactors, MESFETs or PIN diodes [1–3] are used. Nevertheless, these components have an important insertion loss level and low isolation which yield many difficulties in the design of devices, especially filters. There are also other tuning technics using functional material-based components such as ferroelectric varactors [4], liquid crystal [5] or ferromagnetic material [6]. Nevertheless, such components suffer from long switching time and power consumption. Moreover, they need bulky actuation sources with high voltage or current to apply electromagnetic field.

*Received 14 February 2012, Accepted 18 March 2012, Scheduled 24 March 2012*

* Corresponding author: Thanh Mai Vu (tmprigent@laplace.univ-tlse.fr).

Microelectromechanical systems (MEMS) technology have demonstrated great potentialities for many applications and mainly for high frequency applications due to their low-power consumption, low loss, excellent linearity and facility to be implemented with microwave integrated circuit (MIC) through passive fabrication techniques [7, 8]. Thus, the purpose is to replace the current active components in systems by passive components (MEMS).

This paper presents a topology of a cantilever which is used in a tunable resonator from W-frequency band (94 GHz) to V-frequency band (60 GHz) [9]. The self-matched tunable resonator solution developed hereafter has been synthesized considering the $C_{\text{up}}$ and $C_{\text{down}}$ values for MEMS [10]. Thus, MEMS has to be designed to fit with criteria in the synthesis.

The MEMS switch is realized on Si-BCB (Silicon-Benzocyclobuten) technology which appears as one of the possible technologies due to its good electrical characteristics at very high frequency [11]. In this paper, a study of MEMS electrical and mechanical properties is presented so as to explain the choice of MEMS configuration. MEMS simulation, fabrication as well as characterization are then presented. Preliminary results of this study were presented in [12].

## 2. MEMS DESIGN FOR RF APPLICATION

### 2.1. RF MEMS Topology

From the demand of the switch in tunable resonator synthesis, MEMS is used to change the lines lengths in a resonator [10]. A topology of an inline MEMS switch is chosen to facilitate MEMS integration in the circuit. In this case, the application varies from W-band to V-band, cantilever dimension and its capacitance values at up- and down-state need to satisfy specific conditions: the MEMS has to possess an upstate capacitance value as small as possible and a downstate capacitance value as high as possible ($C_{\text{down}}/C_{\text{up}}$ is chosen higher than 60 in the synthesis). Two types of cantilever are investigated: capacitive switch (metal — insulator — metal contact) and DC contact switch (metal — metal contact) (Figure 1).

#### *2.1.1. Upstate Capacitance Value*

The upstate capacitance value of a capacitive contact can be calculated as follows:

$$C_{\text{air}} = \frac{\varepsilon_0 S}{g_{\text{air}}} \tag{1}$$

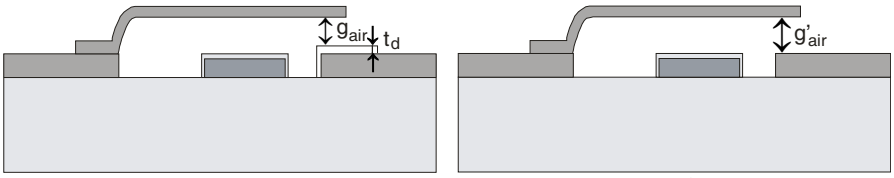


**Figure 1.** Cantilever topology (a) capacitive switch, (b) DC contact switch

$$C_d = \frac{\varepsilon_0 \varepsilon_r S}{t_d} \tag{2}$$

$$C_{\text{up}} = \frac{C_{\text{air}} \cdot C_d}{C_{\text{air}} + C_d} = \frac{\varepsilon_0 S}{g_{\text{air}} + \frac{t_d}{\varepsilon_r}} \tag{3}$$

with $S$ the contact area, $\varepsilon_0$ the electric constant, $g_{\text{air}}$ the height of air gap, $t_d$ the dielectric thickness and $\varepsilon_r$ relative dielectric constant.

In the case of DC contact, upstate capacitance value is given by:

$$C_{\text{up}} = C_{\text{air}} = \frac{\varepsilon_0 S}{g'_{\text{air}}} \tag{4}$$

So, for the same contact area, the gap height of a capacitive contact $g_0 = g_{\text{air}} + t_d/\varepsilon_r$ is smaller than the ones of a DC contact $g'_0 = g'_{\text{air}} = g_{\text{air}} + t_d$. Therefore, DC contact switch gives a smaller upstate capacitance value than capacitive contact switch.

#### *2.1.2. Downstate Capacitance Value*

In the downstate position, the capacitive switch results in a capacitance $C_{\text{down}}$ whereas the ohmic switch results in a contact resistance $R_c$ and an infinite capacitance which corresponds to the desired operating mode. From these observations, the inline DC contact MEMS series switch is the most suitable for our application.

### 2.2. RF MEMS Modeling

#### *2.2.1. Inline DC Contact MEMS Series Switch Conception*

The general circuit model for this type of MEMS is presented in Figure 2.

The upstate capacitance is composed of a series capacitance ($C_s$) between the transmission-line and the cantilever, and a parasitic capacitance ($C_p$) between the open-ends of the transmission-line [13].

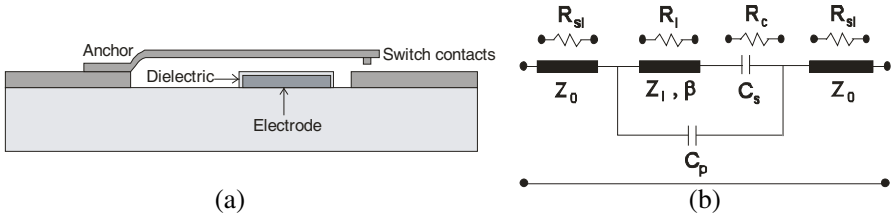


**Figure 2.** Cantilever. (a) Topology, (b) circuit model.

The total upstate capacitance of an inline switch with one contact area is given by:

$$C_u = C_s + C_p \tag{5}$$

The downstate resistance is composed of a DC contact resistance ($R_c$), the resistance of cantilever ($R_l$) and resistances on the transmission-line ($R_{sl}$). The total switch resistance for an inline switch with one contact area is:

$$R_s = R_c + 2R_{sl} + R_l \tag{6}$$

For a good contact between cantilever and transmission-line, dimples are used. Moreover, to eliminate the stiction problem between the bottom metal of cantilever and electrode, a thin layer of silicon nitride $Si_3N_4$ is used to cover the electrode. An array of holes is created on the bottom metal to reduce the squeeze film damping [14] and to facilitate the final releasing step of fabrication. The contact resistance depends on the size of the contact area, the mechanical force applied, and the quality of the metal-to-metal contact. Three contact fingers were used to reduce the overall contact resistance of the switch and to divide the RF/DC current [15]. Then MEMS electrode should be correctly placed in order to ensure a pull-down voltage lower than 100 V which is the highest actuation voltage available in our measurement test bench for circuits at 94 GHz.

### *2.2.2. Mechanical Concept for MEMS Dimension*

Figure 3 shows the chosen geometry of the cantilever with its dimensions: beam width $w$, length of electrode $W$, height of air gap between the electrode and the movable beam $g_{\text{air}}$, dielectric thickness $t_d$ and beam thickness $t$.

Let us start by determining the influence of cantilever dimensional parameters: spring constant $k$ and the actuation voltage $V_p$.

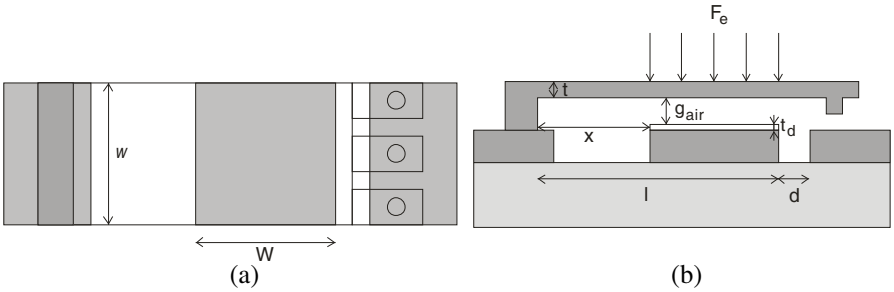


**Figure 3.** Geometric parameters of cantilever definition.

The equation of the actuation voltage:

$$V_p = \sqrt{\frac{8k}{27\varepsilon_0 W w}\left(g_{\text{air}} + \frac{t_d}{\varepsilon_r}\right)^3} \tag{7}$$

with $k$ the cantilever stiffness or spring constant:

$$k = 2Ew\left(\frac{t}{l}\right)^3 \frac{1-\left(\frac{x}{l}\right)}{3-4\left(\frac{x}{l}\right)^3+\left(\frac{x}{l}\right)^4} \tag{8}$$

where $x$ is the distance from the cantilever anchor to the first point of applied force and $l$ is the distance from the anchor to the last point of applied force.

In our case, the movable beam has no contact with the electrode but provides a force at the end of the cantilever. In these conditions, $x = l$ and the spring constant becomes:

$$k = 3\frac{EI}{l^3} \tag{9}$$

where $I$ is the moment of inertia defined by:

$$I = w \cdot \int z^2 \cdot dz = \left|\frac{w \cdot z^3}{3}\right|_{-\frac{t}{2}}^{+\frac{t}{2}} = \frac{w \cdot t^3}{12} \tag{10}$$

So,

$$k = 3\frac{EI}{l^3} = \frac{Ew}{4}\left(\frac{t}{l}\right)^3 \tag{11}$$

The cantilever's mechanical resonant frequency is:

$$f_0 = \frac{1}{2\pi}\sqrt{\frac{k}{m}} \tag{12}$$

where $m$ is the effective mass: $m = 0.35(lwt)\rho$, $\rho$ is the mass density.

The quality factor of cantilever is defined as:

$$Q = \frac{\sqrt{E\rho} \cdot t^2}{\mu A^2} g_0^3 \tag{13}$$

with $A = W \cdot w$, $g_0$ the gap height, $\mu$ the coefficient of viscosity, $\mu = 1.2566 \cdot 10^{-6} \cdot \sqrt{T} \cdot (1 + \frac{110.33}{T})^{-1}$ kg/m·s (in case of ideal gas), $T$ is in Kelvin.

The switching time depends on the quality factor:

- If Q $\geq$ 2:

$$t_s \approx 3.67 \frac{V_p}{V_s \cdot \omega_0} \tag{14}$$

where $V_p$ is the actuation voltage and $V_s$ is the applied voltage ($V_s = 1.2 - 1.4V_p$).

- If Q $\leq$ 0.5:

$$t_s \approx \frac{9V_p^2}{4\omega_0 Q V_s^2} \tag{15}$$

From these equations, we analyze the choice of dimensional parameters:

- *Choice of cantilever width w:* The width of cantilever linearly affects the spring constant, it must be large enough to ensure a high rigidity of the MEMS beam.

- *Choice of electrode length W:* According to Equations (7) and (11), for a fixed electrode length ($W$), a change in the electrode position ($l$) introduces a modification in actuation voltage. Indeed, in Figure 4 one can observe that for $W$ fixed, the more the distance $d$ grows (or $l$ decreases), the more the spring constant $k$ increases and the more the actuation voltage $V_p$ increases. Therefore, $d$ should be as small as possible. Due to technological constraints, the dimension $d$ is fixed to 10 µm which is the lowest achievable slot dimension.

Once $d$ is chosen, one needs to determine the electrode length. Figure 5 illustrates the evolution of the spring constant and actuation voltage versus the electrode length ($W$).

We can see that to reduce actuation voltage, electrode length should be as long as possible. Thus, as illustrated in Figures 6(a) and 6(b), for $x_2 < x_1$, it results $V_{p2} < V_{p1}$. However, since the electrode length is important (Figure 6(c)), an electrostatic force in the vicinity of the anchor tends to increase the mechanical restoring force $F_r$. Thus a higher electrostatic force on the beam is obtained. This phenomenon can curl the beam up which will deteriorate the metal to metal contact quality. So, one has to limit this length to conserve a good electric contact while minimizing actuation voltage.

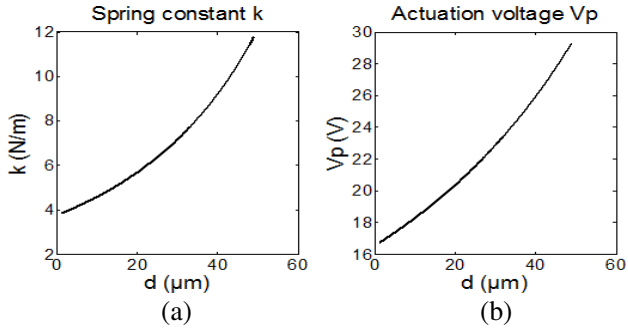


**Figure 4.** Spring constant $k$ (a) and actuation voltage $V_p$ (b) variation vs. $d$.

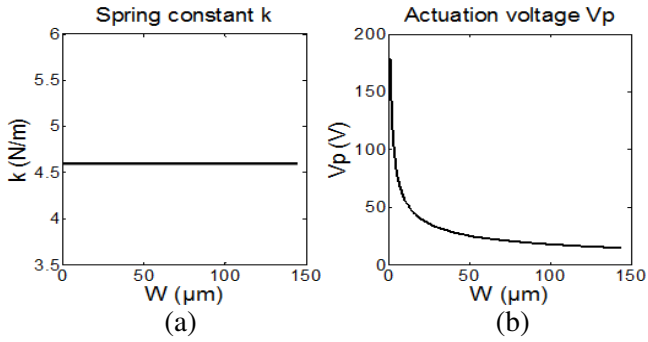


**Figure 5.** Spring constant $k$ (a) and actuation voltage $V_p$ (b) variation vs. $W$.

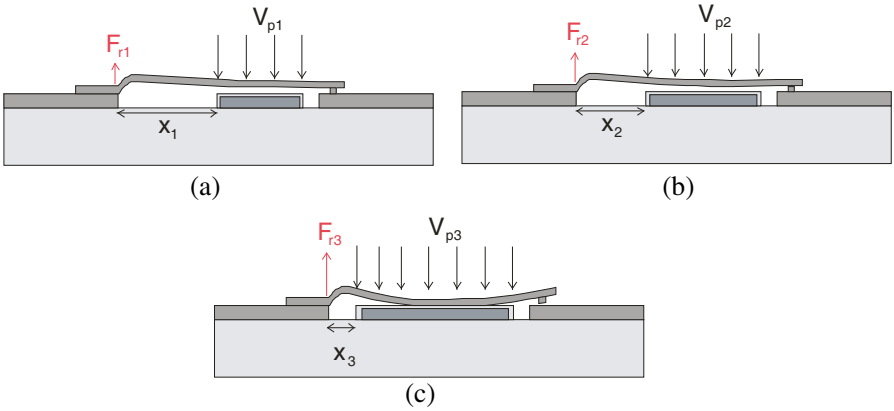


**Figure 6.** Cantilever deformation in term of distance $x$.

- *Choice of beam thickness t:* The beam stiffness is proportional to beam thickness ($t^3$) whereas actuation voltage is proportional to $t^{3/2}$. Thereby, a small value of $t$ reduces the actuation voltage $V_p$ but it has to be limited to maintain a sufficient beam stiffness $k$.

- *Choice of the initial gap height* $g_0$ ($g_0 = g_{\text{air}} + t_d$): One can see that for a small value of $g_0$, the actuation voltage decreases. However, in order to ensure sufficient contact- and a mechanical restoring-force as well as to facilitate the releasing technological process of sacrificial photoresist, the gap height should not be less than 3 µm. The dielectric thickness $t_d$ should be sufficient to prevent stiction problem while being thin enough to ensure a good contact.

Based on this analysis, the cantilever geometric parameters are chosen as follows: $w = 90\,\mu\text{m}$; $W = 95\,\mu\text{m}$; $d = 10\,\mu\text{m}$; $x = 50\,\mu\text{m}$; $t = 2\,\mu\text{m}$, $g_0 = 3\,\mu\text{m}$, $t_d = 0.4\,\mu\text{m}$. With the gold Young modulus $E = 78000\,\text{MPa}$, $\varepsilon_0 = 8.854 \cdot 10^{-12}$, the calculated actuation voltage is: $V_p \approx 16.6\,(\text{V})$ and spring constant is : $k \approx 3.8\,(\text{N/m})$. The mechanical resonant frequency is $f_0 \approx 711\,\text{KHz}$. In this case, the quality factor is $Q \approx 0.043 < 0.5$, so the switching time is calculated from Equation (15) $t_s \approx 8.1\,\mu\text{s}$.

## 3. TECHNOLOGY FOR MEMS IMPLEMENTATION

Technologies on silicon offer an interest with respect to cost reduction and the integration of active functions. Nevertheless their major drawback is that levels of dielectric loss are not compatible with the specifications required for passive functions, especially in this frequency range. An alternative consists in the use of Si-based technologies. Si-BCB technology is chosen due to its low cost first, then its good electric properties in millimetre frequency range.

At 94 GHz, the BCB coating has a dielectric constant of about 2.65 and a dissipation factor of 0.002 instead of 11.8 and 0.018 respectively for the silicon. Moreover, in this frequency range, BCB layer should be as least 20-µm-thick in order to reduce the insertion losses [11, 16]. TFMS (Thin Film Microstrip) technology is addressed for the choice of Si-BCB technology. Figure 7 describes a TFMS transmission line with CPW access realized using via holes for on-wafer measurements.

## 4. MEMS SIMULATION

The structure was designed and simulated using 3D electromagnetic software HFSS which is one of the most reliable for analysing electromagnetic effect in millimetre field. So, MEMS is designed on a 20 µm-BCB substrate. Its movement from upstate to downstate is

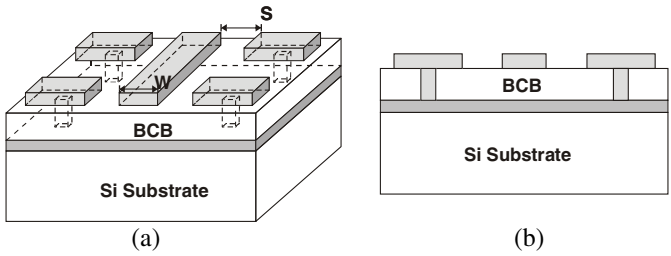


**Figure 7.** TFMS technology: Transmission lines with CPW access.

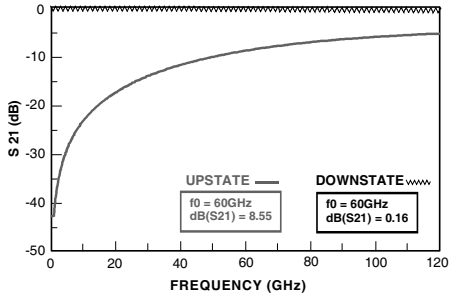


**Figure 8.** MEMS transmission parameters electromagnetic simulation.

controlled using a variable "state" which changes from 0 (for upstate position) to 1 (for downstate position). However, HFSS simulation just allows us to calculate S parameters but not the contact resistance. So we can just calculate the global resistance which is composed of contact loss and cantilever loss extracted from $S$ parameters. In DC contact switch, the global resistance is dominated by the contact resistance [13], according to the low length of our MEMS compared to the wavelength, global and contact resistances are almost the same.

From this simulation, one can calculate the total upstate capacitance and downstate global resistance via isolation and insertion loss:

$$S_{21} = \frac{2j\omega C_u Z_0}{1 + 2j\omega C_u Z_0} \tag{16}$$

$$\text{Loss} = 1 - |S_{11}|^2 - |S_{21}|^2 = \frac{R_s}{Z_0} \tag{17}$$

Figure 8 describes transmission parameter ($S_{21}$) obtained by HFSS for up- and down-state of an inline DC-contact MEMS series switch on a 20-µm BCB. At 60 GHz, the upstate isolation is 8.55 dB and the

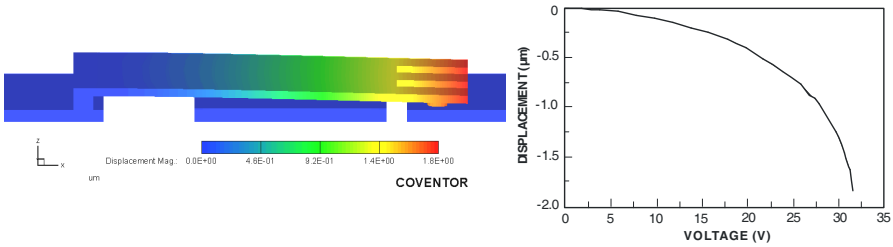


(a) (b)

**Figure 9.** (a) MEMS simulation (Coventor), (b) voltage for MEMS displacement.

downstate insertion loss is 0.16 dB. The upstate capacitance calculated by HFSS is 9.5 fF and the downstate global resistance of 1.1 Ω is achieved with the inline switch.

## 5. ELECTROMECHANICAL SIMULATION

For this structure of MEMS, the pull-down voltage has to be designed below the maximum voltage that can be used by the test bench. Therefore electro-mechanical behaviour of the structure has been evaluated using CoventorWare to calculate the actuation voltage. CoventorWare is a well suited software tool for designing and analyzing MEMS structure. It allows us to evaluate the effect of design parameters on contact, restoring forces and actuation voltage. Moreover, one of its interest is to provide a better understanding of technological process influences when designing structure. By using Coventor, the actuation voltage obtained is 32 V for a contact between dimples and transmission line (Figure 9).

## 6. MEMS FABRICATION

The fabrication process of RF MEMS switch composes of eight main steps which are described as follows (Figure 10):

1) First the ground plan of microstrip is realized using a Ti/Au seed layer deposited by evaporation prior to gold electroplating.
2) The via-holes are then deposited by 20-µm-thick gold electroplating in a thick photoresist mould.
3) Next step consists in BCB deposition. A 300Å thin film of titanium is first evaporated in order to improve adhesion of BCB layer on gold [17]. 20-µm-thick BCB layer is then deposited. The

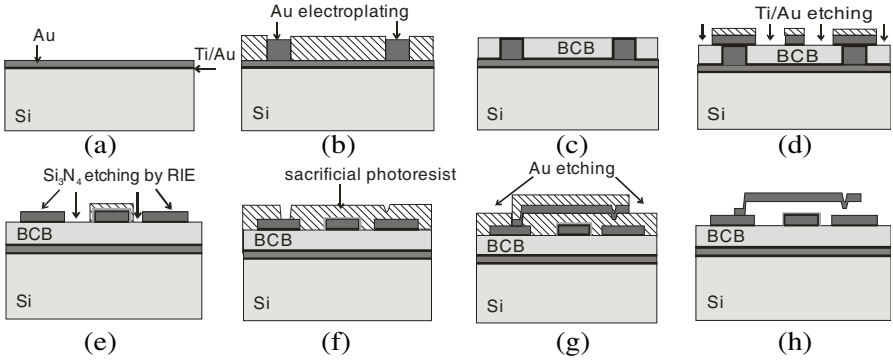


**Figure 10.** MEMS fabrication process on Si-BCB technology.

polymer is then hard-cured at 250°C. Next step consists in an oxygen plasma descuming to eliminate residues left from the BCB deposition.

4) The microstrip is then elaborated in a similar way as the ground plane metallization. Nevertheless, at this time Ti/Au evaporation should be realized at 150°C to enhance adhesion of gold on BCB layer. The seed layer Ti/Au between lines is then removed by chemical etching.

5) Next step is to realize dielectric layer on the electrode. A 500 Å-thick Ti layer is first evaporated on the electrode to improve adhesion of dielectric layer on gold. The 400 nm-thick $Si_3N_4$ layer is then deposited by plasma-enhanced chemical vapor deposition (PECVD). The dielectric layer out of the electrode is etched by reactive ion etching (RIE).

6) Once the dielectric layer is patterned on the electrode, a photoresist mould is deposited for gap filling and then two sacrificial photoresist layers are elaborated which form cantilever (growth of anchors and dimples).

7) Cantilever metallization is deposited by 100 nm-thick gold evaporation followed by 1.9 µm-thick Au electroplating and then gold etching.

8) The final step consists in releasing the switch. The sacrificial layer is removed using successive chemicals baths and the structure is dried by CO2 critical point drying system.

A photograph of the MEMS achieved with such a technological process is presented in Figure 11.

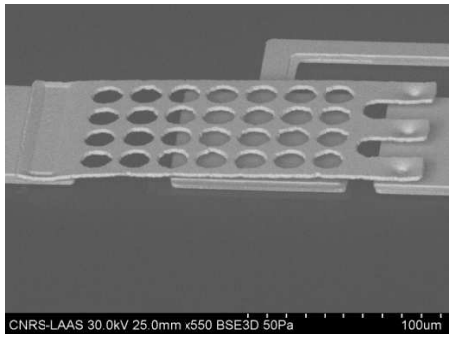


**Figure 11.** MEMS inline switch (SEM).

## 7. MEMS CHARACTERIZATION

### 7.1. *S*-parameter Measurements

For this cantilever model, we are interested in the isolation level in the upstate and insertion loss level in the downstate. The measurements were done using Vector Network Analyser ME7808A for $S$ parameters from 10 MHz to 110 GHz. Measurements were performed using on-wafer short-open-line-thru (SOLT) calibration kit as well as thru-reflection-line (TRL) method. Both of these two methods give the same results (Figure 12).

The experimental results show an upstate isolation of 15.10 dB and a downstate insertion loss of 1.23 dB at 60 GHz. The measured isolation is greater than the expected one (obtained by simulation).

### 7.2. Actuation Voltage Measurements

Reliability measurements were made with Anritsu 37369C Vector network analyser from the RF MEMS Reliability Test Bench under room environment conditions (23.6°C, 43% humidity). This bench set allows us to determine electromechanical parameters of cantilever, such as Pull-in/Pull-out voltages. Experimental results show a Pull-in voltage around 80 V and Pull-out (release) voltage in the range of 40 V (Figure 13).

This high actuation voltage can be explained by the cantilever beam curling in the upstate position after fabrication process. Figure 14 shows that the MEMS gap height obtained is 3.7 μm instead of 1.5 μm as predicted.

This problem comes from stress gradient ($\sigma$) over the cantilever beam [13]. This stress gradient depends on deposition conditions

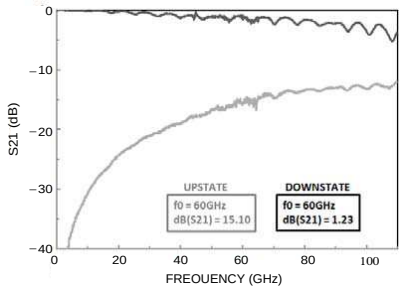


**Figure 12.** MEMS transmission parameters measurements.

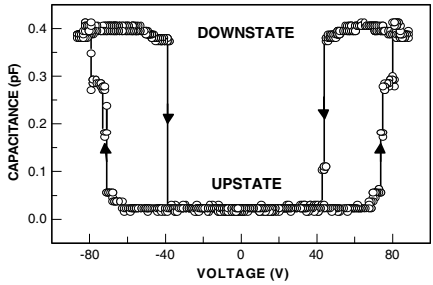


**Figure 13.** Cantilever pull-in and pull-out voltages.

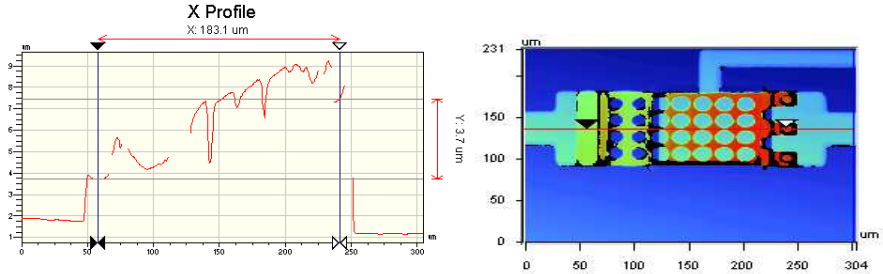


**Figure 14.** Cantilever profill.

and material composition of the beam. In the sacrificial photoresist releasing process, the stress gradient is released in the beam and generates a moment which deflects the tip of cantilever upon the contact area. The deflection at the tip of the cantilever due to stress gradient can be expressed as:

$$\Delta z = \frac{M \cdot l^2}{2 \cdot E \cdot I} \tag{18}$$

with $M$ the bending moment as a function of the dimensions of the beam:

$$M = -\frac{1}{6} w \cdot t^2 \cdot \sigma \tag{19}$$

and $I$ the moment of inertia is defined in Equation (10).

In this case, $\Delta z = 3.7 - 1.5 = 2.2\,\mu\text{m}$, so the stress gradient $\sigma$ calculated here is equal to 14.28 MPa. To reduce this curling phenomenon, one should replace the sacrificial photoresist layer (AZ5214) so that $\sigma$ is around 1–5 MPa, the use of PMGI photoresist seems to be an interesting alternative [18].

### 7.3. Cycling Test

This test is realized by periodically switching the cantilever while controlling component microwave performances. Cantilever activation can be achieved with different signals at different frequencies.

In this case we use square signal and activation is realized from 40 GHz to 110 GHz. Figure 15(a) illustrates the transmission parameters ($S_{21}$) at up- and down-state position before cycling. In the downstate, we observed a resonance at 105 GHz, which comes from the inductor introduced by the cantilever resonating with parasitic capacitors. Figure 15(b) shows the cantilever cycling test using oscilloscope supplying 80 V amplitude square signal with a 50 Hz frequency.

After 800000 cycles, the performances obtained do not vary. Figures 16(a) and 16(b) show the magnitude difference of $S_{21}$ parameters before and after cycling in the up- and down-state position.

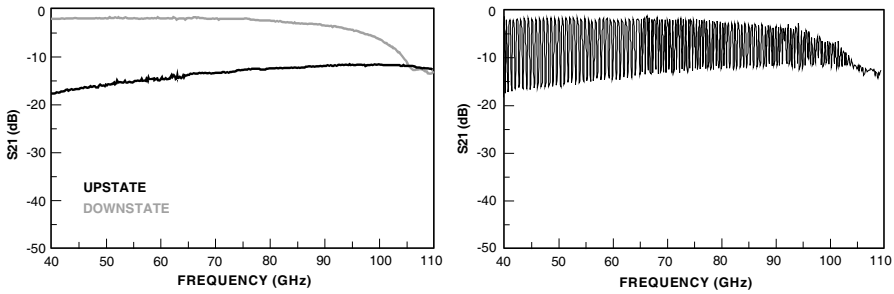


**Figure 15.** Cycling test (a) before switching, (b) MEMS switching.

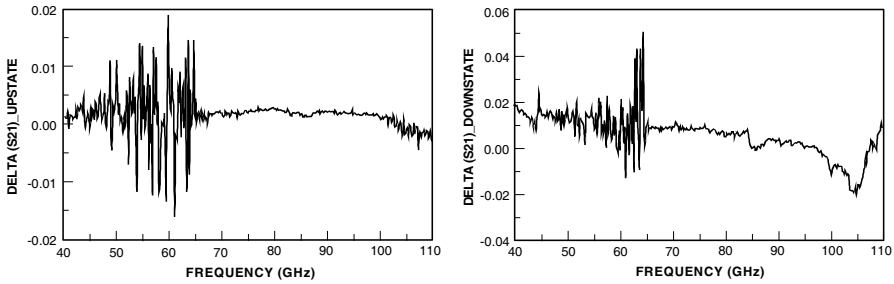


**Figure 16.** Magnitude difference of $S_{21}$ parameters before and after cycling in (a) upstate, (b) downstate.

This performance can be explained by MEMS dimensions choices which allow a low actuation voltage while maintaining a sufficient spring constant. Indeed it introduces a mechanical force for a convenient DC contact while limiting the gold contact deterioration. Moreover, MEMS configuration with three contact fingers ensures a good DC contact whatever the quality of gold contact is.

## 8. CIRCUIT IMPLEMENTATION

This MEMS switch has ever been integrated in tunable resonator called modified — DBR [10] and fabricated on the same process. Three MEMS are placed in three stubs (Figure 17(a)) to control its lengths. The middle stub allows us to control center frequency from 94 GHz to 60 GHz while two others stubs control the low- and high-frequency transmission zeros. Figures 17(b) and 17(c) show the results obtained when MEMS are fixed at up- and down-states in the resonator.

We can see that in the upstate, there is a 6 GHz frequency shift between experiments and simulations due to curling phenomenon.

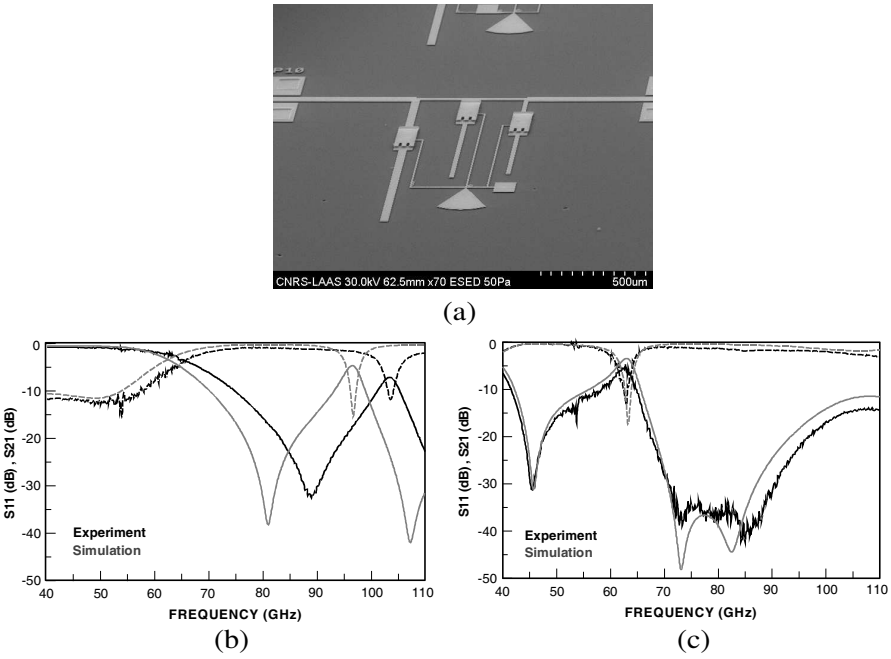


**Figure 17.** MEMS integration in tunable resonator (a) and $S$ parameters in (b) up- and (c) down-states.

This phenomenon causes an upstate capacitance value smaller than the expected one, which results in a frequency shift toward higher frequency. However, the tunable resonator presents an important excursion in frequency.

This circuit is just a test for MEMS integration so in upstate there is still a transmission at 60 GHz which comes from the out-of-band response of the DBR resonator. The aim of this circuit is to demonstrate the efficiency of both technological process for MEMS and synthesis for filter. Therefore, a resonator was developed so as to highlight these aspects for a wide frequency-range tunable resonator. For typical applications such tenability is limited to 10%. The out-of-band response limits the use of such a structure to 70 GHz for the lowest frequency. So it is much more interested to use this structure for automotive radar systems or radio astronomy/passive sensing applications [19] where a tunable filter from 77 GHz to 94 GHz is required.

## 9. CONCLUSION

A DC-contact MEMS switch for tunable resonator from W-band to V-band was designed and fabricated in TFMS Si-BCB technology. Despite of curling phenomenon, the cantilever shows very good RF performances in terms of isolation and insertion loss at 60 GHz even after 800000 switching cycles. Performances obtained for tunable resonator from W-band (94 GHz) to V-band (60 GHz) attest from technological process quality as well as the concepts presented here.

## REFERENCES

1. Brown, R. and G. M. Rebeiz, "A varactor tuned RF filter," *IEEE Transactions on Microwave Theory and Techniques*, Vol. 48, 1157–1160, July 2000.
2. Tanné, G., E. Rius, F. Mahé, S. Toutain, F. Biron, L. Billonnet, B. Jarry, and P. Guillon, "Improvement in losses and size of frequency tunable coplanar filter structures using MMIC negative resistance chips for multistandard mobile communication systems," *IEEE MTT-S Int. Microwave Symp. Dig.*, 1165–1168, Boston, MA, 2000.
3. Hong, J. S., "Reconfigurable planar filters," *IEEE Transactions on Microwave Theory and Techniques*, Vol. 10, No. 6, 73–83, October 2009.

4. Nath, A. J., D. Ghosh, W. Fathelbab, J. P. Maria, A. I. Kingon, P. D. Franzon, and M. B. Steer, "A tunable combline bandpass filter using barium strontium titanate interdigital varactors on an alumina substrate," *IEEE MTT-S Int. Microwave Symp. Dig.*, 595–598, June 2005.
5. Bernigaud, J. F., N. Martin, P. Laurent, C. Quendo, G. Tanne, B. Della, F. Huret, and P. Gelin, "Liquid crystal tunable filter based on DBR topology," *36th European Microwave Conference*, 368–371, September 2006.
6. Tsutsumi, M. and T. Fukusako, "Magnetically tunable superconducting microstrip resonators using yttrium iron garnet single crystals," *IEEE MTT-S Int. Microwave Symp. Dig.*, Vol. 3, 1491–1494, June 1997.
7. Rebeiz, G. M. and J. B. Muldavin, "RF MEMS switches and switch circuits," *IEEE Microwave Mag.*, 59–71, December 2001.
8. Dussopt, L. and G. M. Rebeiz, "High-Q millimeter-wave MEMS varactors: Extended-tuning range and discrete-position designs," *IEEE Microwave Theory and Technique Symposium*, 1205–1208, Phoenix, 2002.
9. Vu, T. M., G. Prigent, and R. Plana, "MEMs based reconfigurable dual behavior resonator using BCB technology in W-frequency range," *IEEE International Newcas Taisa Joint Conference*, July 2009.
10. Prigent, G., T. M. Vu and R. Plana, "Synthesis for tunable dual behavior resonator," *IEEE Asia Pacific Microwave Conference*, 123–126, December 2009.
11. Grenier, K., D. Dubuc, L. Mazenq, J. P. Busquere, B. Ducarouge, F. Bouchriha, A. Rennane, V. Lubecke, P. Pons, P. Ancey, and R. Plana, "Polymer based technologies for microwave and millimeterwave applications," *IEEE International Electron Devices Meeting*, 545–548, December 2004.
12. Vu, T. M., G. Prigent, J. Ruan, A. Rumeau, P. Pons, and R. Plana, "Fabrication and characterization of RF-MEMS switch in V-band," *IEEE Asia Pacific Microwave Conference*, 202–205, December 2009.
13. Rebeiz, G. M., *RF MEMS Theory, Design, and Technology*, J. Wiley & Sons, Hoboken, New Jersey, 2003.
14. Mihailovich, R. E., M. Kim, J. B. Hacker, E. A. Sovero, J. Studer, J. A. Higgins, and J. F. DeNatale, "MEM relay for reconfigurable RF circuits," *IEEE Microwave and Wireless Components Letters*, Vol. 11, No. 2, 53–55, February 2001.

15. Zacvracky, P. M., N. E. McGruer, R. H. Morrison, and D. Potter, "Microswitches and microrelays with a view toward microwave applications," *Int. J. RF Microwave CAE*, Vol. 9, No. 4, 338–347, 1999.
16. Prigent, G., E. Rius, F. Le Pennec, S. Le Maguer, C. Quendo, G. Six, and H. Happy, "Design of narrow-band DBR planar filters in Si-BCB technology for millimeter-wave applications," *IEEE Transactions on Microwave Theory and Techniques*, Vol. 52, No. 3, 1045–1051, March 2004.
17. Six, G., G. Prigent, E. Rius, G. Dambrine, and H. Happy, "Fabrication and characterization of low-loss TFMS on silicon substrate up to 220 GHz," *IEEE Transactions on Microwave Theory and Techniques*, Vol. 53, No. 1, 301–305, January 2005.
18. Villeneuve, C., S. Aouba, M. Dilhan, D. Bourrier, P. Pons, and R. Plana, "Low stressed gradient in gold micromachined cantilevers," *20th Micromechanics Europe Workshop*, September 20–22, 2009.
19. Chang, H.-Y., J.-H. Tsai, T.-W. Huang, H. Wang, Y. X. Xia, and Y. H. Shu, "A W-band high-power predistorted direct-conversion digital modulator for transmitter applications," *IEEE Microwave and Wireless Components Letters*, Vol. 15, No. 9, 600–602, September 2005.